ACS OMEGA

http://pubs.acs.org/journal/acsodf

Article

Photoionization Spectroscopic and Theoretical Study on the Molecular Structures of *cis*- and *trans*-3-Chlorothioanisole

Zhe Zhang, Yikui Du,* Gao-Lei Hou,* and Hong Gao*

Cite This: *ACS Omega* 2022, 7, 8456−8465

Read Online

ABSTRACT: Resonance-enhanced two-photon ionization (R2PI) and mass-analyzed threshold ionization (MATI) spectra are measured for the *cis*- and *trans*-3-chlorothioanisole (3ClTA). The first electronic excitation energy (E_1) and the adiabatic ionization energy (IE) of the *cis*-rotamer are determined to be 33 959±3 and 65 326±5 cm^{-1}, respectively, and those of the *trans*-rotamer are determined to be 34102±3 and 65 471±5 cm^{-1}, respectively. Density functional theory (DFT) calculations confirm that both the *cis*- and *trans*-rotamers of 3ClTA are stable and coexist in their respective S_0, S_1, and D_0 states. Both rotamers adopt planar structures with *cis*- being slightly more stable than *trans*- in the respective S_0, S_1, and D_0 states. The conformation, substitution, and isotope effects on the molecular structure, active vibrations, and electronic transition and ionization energies of 3ClTA are analyzed.

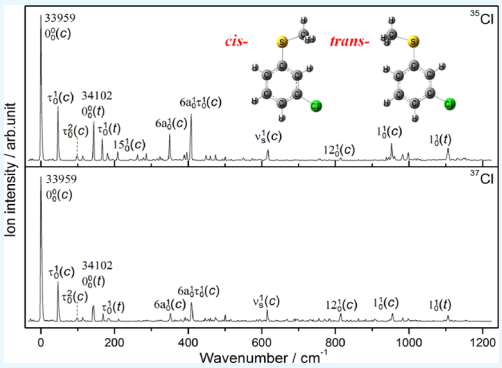

1. INTRODUCTION

There have been numerous experimental and theoretical studies for investigating the stable structures and properties of anisole and thioanisole (TA) derivatives in their respective electronic ground (S_0), first excited (S_1), and cationic ground (D_0) states.[1−9] Due to strong conjugation effect between the benzene ring and the substituent functional groups, most of those molecules are found to be planar. However, several exceptions have been observed. For example, a nonplanar stable structure was observed for *trans*-2-fluoroanisole (2-F anisole) in its S_0 state with Fourier transform infrared (FTIR) spectroscopy[10] and a small structure tilt was observed for *trans*-2-fluorothioanisole (2FTA) in its S_1 state through resonance-enhanced two-photon ionization (R2PI) spectroscopy.[11] In 2FTA, the enhanced steric effect and inductive effect caused by the 2-substituted (*ortho*-substituted) F atom play important roles.

For TA derivatives, there exist a lot of controversies, from previous calculations and spectroscopic results,[6,9,12−14] about their stable structures, particularly in their S_1 states. Some theoretical calculations predict their molecular skeletons to be nonplanar in the S_1 state,[12,15] in which the thiomethyl (−SCH_3) group was nearly perpendicular to the benzene ring. The whole molecule has a vertical *gauche*-like structure. This contradicts the general rule that the benzene ring tends to keep a planar structure as favored by π-orbital delocalization.[16] The nonplanar structures obtained by theoretical calculations do not exactly agree with the spectroscopic experiments.[6,9,15] Nevertheless, most TA derivatives have now been determined to be planar or quasi-planar,[6,8,9,12−15] and the competition between the steric effect and the inductive effect caused by −SCH_3 was used to explain the difference between calculations and spectroscopic measurements.[6,9,12] However, the reason for the structure tilt seen in the theoretical calculation is still unclear, and it is worthwhile to investigate the stable structures of halogen-substituted anisole and TA derivatives in various electronic states.

The deformation changes of benzene derivatives upon photoexcitation and photoionization are usually similar to each other for molecules with similar structures.[1,6,16−20] For example, benzene ring is usually enlarged in the S_1 state and a quinoidal structure is often found in the D_0 state. It is reasonable to assume that the conjugation effects of −OCH_3 and −SCH_3 groups with the benzene ring are similar since O and S atoms belong to the same group in the periodic table. Compared with the O atom, the S atom is larger in size, which could make the −SCH_3 group more flexible than the −OCH_3 group.[2,14] Investigation on how the −SCH_3 group substitution affects the molecular properties is limited.

Besides the conjugation effect mentioned above, the steric effect and inductive effect caused by the halogen substitutions should also be considered. For example, the *cis*-rotamer is observed to be stable for 3-fluoroanisole (3-F anisole)[21] but not for 2-F anisole.[10,22] That is due to the fact that the steric effect between the F atom and the −OCH_3 group is weaker in

Received: October 26, 2021
Accepted: February 17, 2022
Published: March 7, 2022

https://doi.org/10.1021/acsomega.1c06003
ACS Omega 2022, 7, 8456−8465

3-substituted (*meta*-substituted) anisole than that in the 2-substituted one. The transition energies (E_1) of Cl-substituted anisoles were found to be red-shifted compared to those of anisole,[23] while those of F-substituted anisoles were found to be blue-shifted.[17,24−26] This is mainly caused by the different inductive effects of F and Cl atoms.

Based on the above discussion, the 3-chlorothioanisole (3ClTA) molecule can be a suitable system for simultaneously comparing the substitution effects between $-SCH_3$ and $-OCH_3$ groups and between Cl and F atoms. To the best of our knowledge, the vibrational spectra of 3ClTA in both S_1 and D_0 states have not been reported, and its structural properties have not been investigated. In this work, we reported a combined theoretical and spectroscopic study on the *cis*- and *trans*-rotamers of 3ClTA. The vibrational spectra of 3ClTA in S_1 and D_0 states were measured by R2PI and mass-analyzed threshold ionization (MATI) spectroscopy. The stable molecular structures and the rotational barriers between the *cis*- and *trans*-rotamers of 3ClTA are calculated by comparing the spectroscopic measurements with the theoretical calculations. The structural changes induced by photoexcitation and photoionization are discussed in detail.

2. RESULTS

2.1. Calculated Results. The chemical structures and the atomic labelings of *cis*- and *trans*-3ClTA are shown in Figure 1.

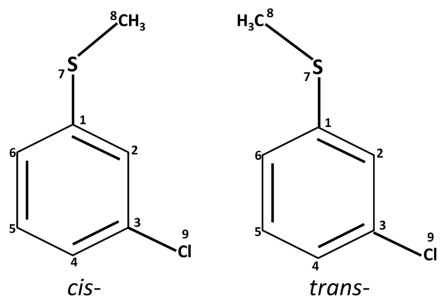

Figure 1. Chemical structures and atomic labelings of (left) *cis*- and (right) *trans*-3ClTA.

The optimized geometric parameters and atomic charges for the two rotamers in S_0, S_1, and D_0 states are listed in Table 1, and their Cartesian coordinates are provided in the Supporting Information (Table S1). The calculated one-dimensional potential energy curves (PECs) of 3ClTA in S_0, S_1, and D_0 states are presented in Figure 2. All PECs were scanned along the C2−C1−S−C8 dihedral angle from −10° to 190° with a 5° increment, and all other structural parameters were optimized without any constraints. The presented energies for the stationary points corresponding to minimum structures include zero-point energy (ZPE) corrections, but ZPE corrections are not included for other points on the PECs.

The calculations indicate that different chlorine isotopes have negligible effects on the investigated properties of 3ClTA, such as molecular geometry, excitation (E_1) and ionization (IE) energies, and vibrational frequencies. Such finding is similar to previous studies on several aromatic molecules containing the chlorine substituent.[1,3,20,23,27,28] Hence, we will focus on the results of the ^{35}Cl-substituted 3ClTA in the following sections for clarity.

The PECs presented in Figure 2 indicate that the *cis*-rotamer of 3ClTA is slightly more stable than its *trans*-rotamer in S_0 and D_0 states, while the calculated energies including ZPE corrections for the stationary points in the S_1 state show that the *trans*-rotamer is slightly more stable than the *cis*-rotamer. Nonetheless, these energy differences are relatively small, and a more confident assignment needs experimental support. In the S_0 state, the calculated energy difference between the *cis*- and *trans*-rotamers is 68 cm^{-1}, including ZPE corrections, and the isomerization energy barrier is about 500 cm^{-1} with respect to the *cis*-rotamer. A previous study showed that flexible organic molecules with interconversion barriers larger than 400 cm^{-1} would not relax significantly during the supersonic expansion.[25] Hence, both the *cis*- and *trans*-rotamers of 3ClTA could exist in the supersonic molecular beam with an estimated population ratio N_{cis}/N_{trans} of about 1.4 according to the Maxwell−Boltzmann distribution under the assumption of thermal equilibrium.

It is noted that in the calculated PEC for the S_1 state (Figure 2), the benzene ring is distorted and the Cl atom is optimized to be out-of-plane for most of the data points, except at the points where the C2−C1−S−C8 dihedral angles are 0 and 180°. Similar behavior has been found previously for the S_1 state of TA.[9,12] Therefore, caution should be taken for quantitative evaluation of the calculated PEC and rotational barrier of 3ClTA in the S_1 state. Nonetheless, at the C2−C1−S−C8 dihedral angles of 0 and 180°, the benzene ring was all optimized to be planar with the Cl atom in the same plane for S_0, S_1, and D_0 states.

A discontinuity at 90° was noted in the PEC of the D_0 state. It is mainly caused by the rotation of the $-CH_3$ group, and such discontinuity does not affect the optimized results for both *cis*- and *trans*-rotamers at 0 and 180° in the D_0 state. Similar discontinuities were observed previously in the PECs of 2-*N*-methylaminopyridine.[26] In this regard, the calculated IEs and relative stabilities of the two rotamers in the D_0 state are assumed to be not affected by the discontinuity at 90°.

2.2. 1C-R2PI Spectra. A typical time-of-flight (TOF) mass spectrum of 3ClTA recorded at the UV wavelength of ∼285 nm is presented in Figure 3. The mass peaks at 159 and 161 amu are assigned, respectively, to the ion signals of ^{35}Cl-3ClTA and ^{37}Cl-3ClTA isotopomers, showing that the mass resolution of the setup is enough for collecting the individual spectra of the two isotopomers of 3ClTA. The 1C-R2PI spectra of the ^{35}Cl and ^{37}Cl isotopomers of 3ClTA in the range of 0−1200 cm^{-1} are shown in Figure 4. Tentative assignments of the observed vibrational features are listed in Table 2, and the Varsányi's labeling system is adopted to approximately describe the observed benzene-like vibrational modes of 3ClTA, which should be classified as an *meta*-di-heavy substituted benzene derivative.[29]

As shown in Figure 4, the first electronic excitation energies of *cis*- and *trans*-^{35}Cl-3ClTA are identical to those of ^{37}Cl-3ClTA, confirming that the Cl isotope substitution has negligible effects on the first electronic excitation energies of 3ClTA. Most of the vibrational frequencies are close to each other for the two 3ClTA isotopomers within 3 cm^{-1}. For example, the $6a_0^1$, ν_s^1, and 1_0^1 bands locate at 349, 617, and 953 cm^{-1} for ^{35}Cl-3ClTA, and 351, 615, and 955 cm^{-1} for ^{37}Cl-3ClTA, respectively. The relative intensities of several vibrational bands are different between the two isotopomers, which is presumably attributed to the edge eliminating effect in choosing the mass range to obtain the reduced spectra during experiments. Those experimentally observed similarities between the two 3ClTA isotopomers verified our predictions

https://doi.org/10.1021/acsomega.1c06003
ACS Omega 2022, 7, 8456−8465

Table 1. Calculated Geometric Parameters and Atomic Charges of *cis*- and *trans*-Rotamers of 3ClTA

	cis-			*trans*-		
	S_0	S_1	D_0	S_0	S_1	D_0
Bond Length (Å)						
S−CH_3	1.815	1.804	1.809	1.815	1.806	1.811
S−C1	1.774	1.754	1.717	1.775	1.754	1.716
C1−C2	1.394	1.395	1.406	1.399	1.412	1.417
C2−C3	1.389	1.434	1.377	1.383	1.431	1.375
C3−C4	1.385	1.401	1.415	1.390	1.389	1.409
C4−C5	1.392	1.390	1.393	1.387	1.402	1.400
C5−C6	1.384	1.440	1.378	1.391	1.433	1.375
C6−C1	1.400	1.403	1.427	1.395	1.389	1.419
C3−Cl	1.755	1.746	1.719	1.754	1.761	1.722
Bond Angle (°)						
C8-S-C1	103.9	106.9	106.7	103.8	106.7	107.2
S-C1-C2	124.1	122.2	125.1	116.0	112.2	114.8
S-C1-C6	116.5	112.9	114.2	124.7	122.9	124.5
C2-C1-C6	119.4	124.9	120.7	119.4	124.8	120.7
C1-C2-C3	119.2	116.0	118.6	119.5	115.6	119.1
C2-C3-C4	122.1	120.7	121.0	121.8	120.9	120.3
C3-C4-C5	118.2	122.0	120.2	118.2	121.9	120.4
C4-C5-C6	121.0	119.0	119.9	121.2	118.7	120.5
C5-C6-C1	120.2	117.5	119.6	119.9	117.8	110.1
C2-C3-Cl	118.6	118.8	120.3	119.0	118.6	120.5
Atomic Charges (*e*)						
H of −CH_3 group	0.208	0.238	0.248	0.207	0.238	0.248
	0.208	0.238	0.248	0.207	0.235	0.248
	0.226	0.233	0.261	0.226	0.233	0.261
C8	−0.705	−0.736	−0.729	−0.704	−0.738	−0.729
S	0.270	0.638	0.668	0.270	0.646	0.681
C1	−0.137	−0.195	−0.170	−0.136	−0.200	−0.169
C2 (H^a)	−0.279	−0.348	−0.241	−0.257	−0.372	−0.199
	(0.218)	(0.208)	(0.240)	(0.222)	(0.212)	(0.248)
C3	0.017	−0.104	0.010	0.014	−0.074	−0.014
C4 (H^a)	−0.251	−0.153	−0.079	−0.250	−0.153	−0.072
	(0.218)	(0.208)	(0.243)	(0.218)	(0.207)	(0.243)
C5 (H^a)	−0.165	−0.281	−0.181	−0.162	−0.301	−0.162
	(0.209)	(0.204)	(0.246)	(0.207)	(0.202)	(0.244)
C6 (H^a)	−0.230	−0.320	−0.117	−0.253	−0.282	−0.161
	(0.210)	(0.203)	(0.239)	(0.205)	(0.192)	(0.229)
Cl	−0.018	−0.031	0.116	−0.015	−0.044	0.104

[a]The H atom in parentheses is directly connected to the C atom before the parentheses.

derived from theoretical calculations, allowing us to discuss only the spectrum of ^{35}Cl-3ClTA in the following sections.

3ClTA has 42 normal modes, and the intensity of the vibronic bands is proportional to the Franck−Condon factors (FCFs), and thus not all vibrational modes, for instance, in the cases of very small FCFs, could be observed in the 1C-R2PI process. The assignments of the observed bands to a specific rotamer have been confirmed by measuring the respective IEs using the MATI spectroscopic method.

According to the calculations, the *cis*-rotamer is slightly more stable than the *trans*-rotamer in the S_0 state and should have a higher population in the supersonic molecular beam and thus corresponds to a stronger band origin peak in the 1C-R2PI spectrum. Hence, the observed vibrational band at 33959 cm^{-1} is tentatively assigned to the *cis*-rotamer's band origin ($S_1 \leftarrow S_0$; 0_0^0 band). This band origin corresponds to E_1. The band at 34102 cm^{-1} is tentatively assigned to the *trans*-rotamer's 0_0^0 band. The experimentally measured 0_0^0 band of the *trans*-rotamer is blue-shifted by 143 cm^{-1} with respect to that of the *cis*-rotamer. These assignments are also consistent with the calculated results that the *cis*-rotamer is more stable than the *trans*-rotamer in the D_0 state. However, these results seem not to be consistent with the calculations in the S_1 state. Such discrepancy could be attributed to the expected difficulty of TDDFT in accurately predicting the electronically excited states.

Besides the 0_0^0 bands, the bands at 46 and 97 cm^{-1} are assigned as the methyl torsion vibrational mode τ_0^1 and its overtone τ_0^2 of the *cis*-rotamer, in good agreement with the calculated methyl torsion vibration of 48 cm^{-1} and its overtone of 96 cm^{-1} (Table 2; also see Figure S1 in the Supporting Information for the vibrational vectors); the band at 209 cm^{-1} is assigned as the *cis*-15_0^1 mode, and the corresponding calculated value is 213 cm^{-1}; the bands at 349, 617, 815, and 953 cm^{-1} are assigned to the in-plane ring deformation modes $6a_0^1$, ν_s^1, 12_0^1, and 1_0^1 of the *cis*-rotamer, also agreeing with the calculated values of 360, 621, 790, and 960 cm^{-1}; and a combination band of $6a_0^1$ and τ_0^1 is observed at 409 cm^{-1}

https://doi.org/10.1021/acsomega.1c06003
ACS Omega 2022, 7, 8456−8465

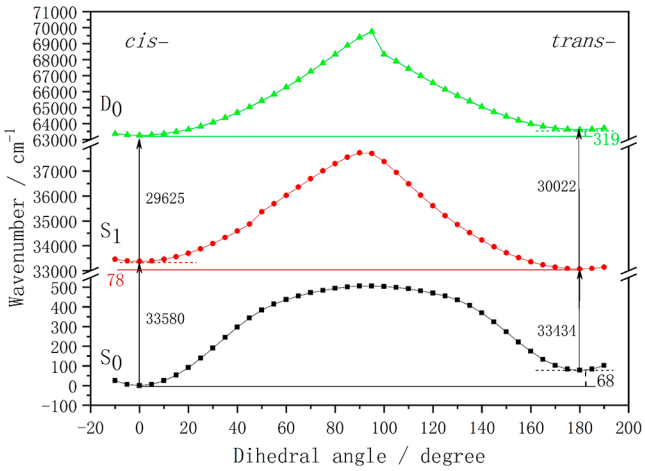

Figure 2. Calculated one-dimensional potential energy curves (PECs) along the dihedral angle between the $-SCH_3$ group and the benzene ring in S_0, S_1, and D_0 states of 3ClTA. The presented energies for the stationary points corresponding to minimum structures include zero-point energy (ZPE) corrections, but ZPE corrections are not included for intermediate points on the PECs.

(Figure 4; the calculated $6a_0^1 + \tau_0^1$ sum frequency is 408 cm^{-1}). As for the *trans*-rotamer, the observed bands at 24 and 41 cm^{-1} are assigned to the methyl torsion mode τ_0^1 and its overtone τ_0^2, and the band at 963 cm^{-1} is assigned to the in-plane ring deformation mode 1_0^1. Those measured values are well reproduced by the calculations, i.e., 33 and 954 cm^{-1} for τ_0^1 and 1_0^1, respectively. The above mode assignments are summarized in Table 2, and in Figure S1 in the Supporting Information, their vibrational vectors are provided.

2.3. MATI Spectra. The MATI spectra and the assignments of the vibrational bands observed for the *cis*- and *trans*-rotamers of ^{35}Cl- and ^{37}Cl-3ClTA are presented in this section. For the *cis*-rotamer, MATI spectra were recorded *via* the vibrational peaks at 0, 46, 349, and 409 cm^{-1}, which show relatively high intensities in the 1C-R2PI spectra; for the *trans*-rotamer, MATI spectra *via* the band origin 0_0^0 at 0 cm^{-1} and the τ_0^1 mode at 24 cm^{-1} were collected. Except for several vibrational peaks that were not observed due to the low intensity, the MATI spectra of ^{37}Cl-3ClTA are nearly identical to those of ^{35}Cl-3ClTA for both rotamers (Figure 5). All vibrational frequencies of the two isotopomers were observed within 7 cm^{-1}, close to the experimental uncertainty (±5 cm^{-1}). Thus, only the MATI spectra of ^{35}Cl-3ClTA are discussed here.

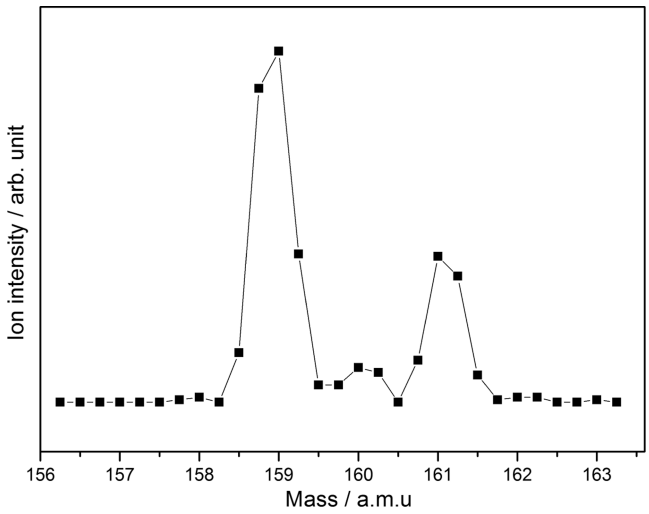

Figure 3. Typical time-of-flight (TOF) mass spectrum of 3ClTA.

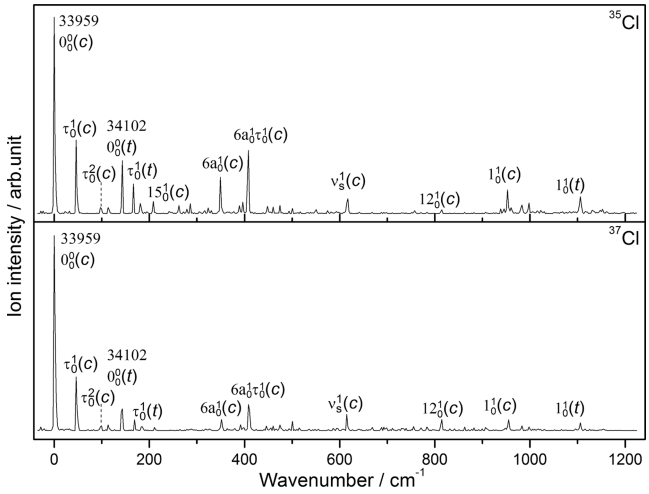

Figure 4. 1C-R2PI spectra of ^{35}Cl-3ClTA (top) and ^{37}Cl-3ClTA (bottom). Letters "*c*" and "*t*" in parentheses represent the *cis*-rotamer and *trans*-rotamer, respectively.

Table 2. Observed Vibrational Frequencies (in cm^{-1}) in the 1C-R2PI Spectra of *cis*- and *trans*-3ClTA and Their Tentative Assignments

cis-3ClTA				*trans*-3ClTA			
exptl.	vib.	theo.[a]	assignment[b]	exptl.	vib.	theo.[a]	assignment[b]
33 959	0		band origin	34 102	0		band origin
34 005	46	48	τ_0^1,torsion	34 126	24	33	τ_0^1,torsion
34 056	97	96[c]	τ_0^2,torsion	34 143	41	66[c]	τ_0^2,torsion
34 168	209	213	15_0^1	35 065	963	954	1_0^1, breathing
34 308	349	360	$6a_0^1$, β(C−C−C)				
34 368	409	408[c]	$6a_0^1\tau_0^1$				
34 576	617	621	ν_s^1, stretching				
34 774	815	790	12_0^1, β(C−C−C)				
34 912	953	960	1_0^1, breathing				

[a]The theoretical values have been scaled by a scaling factor of 0.967. [b]The torsion vibration and stretching vibration are denoted by τ and ν, respectively. The bending mode is designated by β. [c]The calculated frequency for these overtone and combination modes are taken from the sum of the calculated individual frequency of each mode.

https://doi.org/10.1021/acsomega.1c06003
ACS Omega 2022, 7, 8456−8465

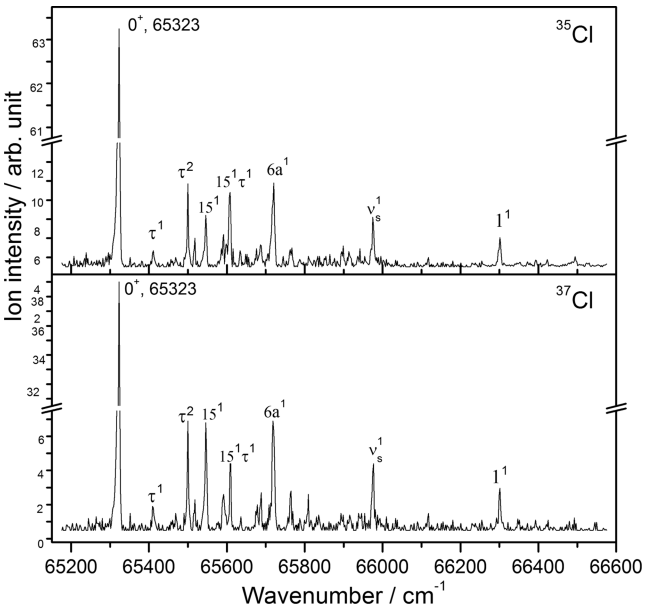

Figure 5. MATI spectra of *cis*-^{35}Cl-3ClTA (top) and ^{37}Cl-3ClTA (bottom) recorded *via* the 0_0^0 vibrational mode in the S_1 state.

As shown in Figures 5 and 6, a strong prominent band origin in the D_0 state was observed for both *cis*- and *trans*-rotamers

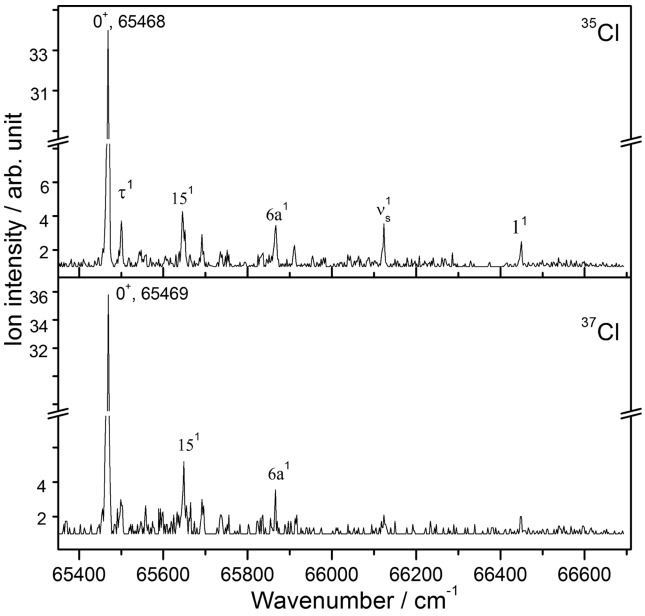

Figure 6. MATI spectra of *trans*-^{35}Cl-3ClTA (top) and ^{37}Cl-3ClTA (bottom) recorded *via* the 0_0^0 vibrational mode in the S_1 state.

via the 0_0^0 vibrational mode in the S_1 state, suggesting that the molecular shapes of both rotamers do not change significantly upon photoionization from the S_1 to D_0 state. The structural change has been quantitatively evaluated by calculating the root-mean-square deviation (RMSD) for distances, and it can be seen that the RMSD values between S_1 and D_0 are 0.029 and 0.123 Å for *cis*- and *trans*-rotamers, respectively (Figure S2). The band origins were measured to be 65 323 and 65 468 cm^{-1} for the *cis*- and *trans*-rotamers, respectively. After correcting the direct-current Stark shift, the IEs of *cis*- and *trans*-rotamers were determined, respectively, to be 65 326±5 and 65 471±5 cm^{-1}, giving a measured difference of IE values to be 145 cm^{-1}. These values agree reasonably with the calculated respective values of 63 205, 63 456, and 251 cm^{-1} including ZPE corrections (Figure 2).

The assignments of all of the vibrational modes observed in the MATI spectra are listed in Table 3. Most of the observed active vibrations are found to be related to the ring deformation and substituent-sensitive modes. For the *cis*-^{35}Cl-3ClTA, the bands at 88 and 177 cm^{-1} are assigned as the methyl torsion vibrational mode τ^1 and its overtone τ^2, respectively. Note that the calculated methyl torsion vibrational frequency is 83 cm^{-1}. The bands at 223, 652, and 980 cm^{-1} are assigned as the vibrational modes of 15^1, ν_s^1, and 1^1, respectively, agreeing with the calculated respective values of 270, 629, and 978 cm^{-1}; the bands at 289 and 446 cm^{-1} are assigned as combination modes. The assignment of the prominent band at 398 cm^{-1} in the MATI spectra *via* the 0_0^0 mode (Figures 5 and 6) is uncertain. It could be due to either the $6a^1$ or $16b^1$ mode. The $6a^1$ mode is observed to be prominent in the 1C-R2PI spectra (Figure 4) with a vibrational frequency of 349 cm^{-1}. This observation seems to support the assignment of the calculated 381 cm^{-1} band to the $6a^1$ mode. However, the vibrational frequency of the $6a^1$ mode is measured to be ∼366 cm^{-1} instead of 398 cm^{-1} in the MATI spectra when the τ_0^1 and $6a_0^1$ modes in the S_1 state were used as the intermediate levels (Figure 7a,b). Similar phenomena have been observed previously for 2FTA.[11] For example, the $6a^1$ band in the D_0 state of 2FTA was observed at 411 cm^{-1} *via* the 0_0^0 mode in the S_1 state, while it was measured to be 400 cm^{-1} when the $\tau_0^2 6a_0^1$ mode was used as the intermediate level. For the *trans*-^{35}Cl-3ClTA, the frequencies of most benzene-ring-related vibrational modes are observed to be close to those of the *cis*-^{35}Cl-3ClTA. The most prominent peak in the MATI spectrum of *trans*-^{35}Cl-3ClTA *via* the methyl torsion mode τ_0^1 at 24 cm^{-1} (Figure 7e) is tentatively assigned as β(C-SCH$_3$) + β(C−Cl), in reasonable agreement with the calculated value of 154 cm^{-1} (Table 3; see also Figure S1 in the Supporting Information for the vibrational vectors). The vibrational frequency for overtone τ^3 should be also close to ∼120 cm^{-1}, while activation of τ^3 is usually highly unfavored.

In Figure 7, MATI spectra *via* several other vibrational bands are presented. It can be seen that when the MATI spectra were recorded *via* the in-plane ring deformation modes $6a_0^1$, ν_s^1, and the combination mode $6a_0^1\tau_0^1$ as the intermediate levels, the most intensive vibrational peaks observed in the MATI spectra correspond to the same modes of the intermediate levels (Figure 7b,d). This indicates that the molecular geometry and the corresponding vibrational coordinates of the $6a_0^1$, ν_s^1, and $6a_0^1\tau_0^1$ modes do not change much upon photoionization from the S_1 state to the D_0 state, as verified by the RMSD analysis (Figure S2). Similar phenomena *via* the benzene-ring-related vibrational levels were previously observed for anisole and its derivatives.[1,17,21,23,30] However, when the methyl torsion mode τ_0^1 was used as the intermediate level, the MATI spectra showed dramatically different characteristics as those *via* the benzene-ring-related vibrational levels. For the *cis*-rotamer, the most prominent peak was due to the 0^+ band, and many other vibrational modes were also significantly excited (Figure 7a). The MATI spectrum of the *trans*-rotamer *via* the methyl torsion mode τ_0^1 at 24 cm^{-1} is completely different from that of the *cis*-rotamer, the 0^+ band was much weaker, and several low-frequency vibrational modes were strongly excited (Figure 7e).

https://doi.org/10.1021/acsomega.1c06003
ACS Omega 2022, 7, 8456−8465

Table 3. Observed Vibrational Frequencies (in cm^{-1}) in the MATI Spectra of the *cis*- and *trans*-Rotamers of 3ClTA and Their Tentative Assignments

cis-							*trans*-			
exptl.							exptl.			
via 0_0^0	*via* 46 cm^{-1}	*via* 349 cm^{-1}	*via* 409 cm^{-1}	*via* 617 cm^{-1}	theo.[a]	assignment[b]	*via* 0_0^0	*via* 24 cm^{-1}	theo.[a]	assignment[b]
0	0	0	0	0			0	0		
88					83	τ^1	34	33	70	τ^1
177	178				166[c]	τ^2		81		τ^2
								127	154	β(C-SCH_3) + β(C−Cl) or τ^3
223	225				270	15^1	177	186	182	15^1
289	310				353[c]	$15^1\tau^1$	223	210	252[c]	$15^1\tau^1$
398	367	366			381	$6a^1$ or $16b^1$	399		400	$6a^1$ or $16b^1$
446	446		441		464[c]	$6a^1\tau^1$				
652				653	629	ν_s^1	655		627	ν_s^1
980					978	1^1	981		968	1^1

[a]The theoretical values have been scaled by a scaling factor of 0.967. [b]The denotations are according to the 1C-R2PI spectra in Table 2, and the torsion vibration and stretching vibration are denoted by τ and ν, respectively. The bending mode is designated by β. [c]The calculated frequency for these overtone and combination modes are taken from the sum of the calculated individual frequency of each mode.

These observations indicate that the methyl torsion mode vibrations are strongly coupled to many other vibrational modes for both the *cis*- and *trans*-rotamers during the photoionization process, but their detailed coupling mechanisms should be quite different due to the different orientations of the $-SCH_3$ groups in the two rotamers (see the torsion mode vibration vectors in Figure S1).

3. DISCUSSION

3.1. Molecular Structures of *cis*- and *trans*-3ClTA in S_0, S_1, and D_0 States.

3.1.1. Molecular Structures in S_0 State. Both *cis*- and *trans*-3ClTA are stable and adopt planar structures possessing a C_s point group in the S_0 state. The *cis*-rotamer is slightly more stable than the *trans*-rotamer, suggesting that the inductive effect of the Cl atom dominates over the steric effect between the two substituent groups in determining the relative stability of the two rotamers. As seen in Table 1, the S−C8 bond in the $-SCH_3$ group is 1.815 Å in the *cis*-rotamer and *trans*-rotamer, and ∠SC1C2 is 124.1° in the *cis*-rotamer and 116.0° in the *trans*-rotamer. The slightly larger ∠SC1C2 in the *cis*-rotamer may arise from the larger steric repelling effect between the Cl atom and the $-SCH_3$ group in the *cis*-rotamer than that in the *trans*-rotamer. This is similar to the larger ∠NC1C2 in *cis*-3-Cl-*N*-methylaniline than that in the *trans*-rotamer.[16]

As for the benzene ring, all of the calculated bond length differences between the two rotamers are less than 0.007 Å and all the bond angle differences are less than 0.4°, indicating that the influences on the structure of the benzene ring caused by the different orientations of the substituent groups in the two rotamers are small.

From the perspective of intramolecular charge distributions, the two rotamers are close to each other. Table 1 shows that their calculated atomic charges in the S_0 state are almost identical, except for the C2 and C6 atoms. The C2 atom is more negative in the *cis*-rotamer (−0.279 *e* for the *cis*-rotamer and −0.257 *e* for the *trans*-rotamer), while the C6 atom is more negative in the *trans*-rotamer (−0.230 *e* for the *cis*-rotamer and −0.253 *e* for the *trans*-rotamer). This could be caused by the electron-donating effect of the $-CH_3$ group, and the C atom closer to the $-CH_3$ group gets more negative charge.

3.1.2. Structural Changes during the $S_1 \leftarrow S_0$ Transition. The intense 0_0^0 bands observed in the 1C-R2PI spectra in Figure 4 suggest that there are only minor geometric changes upon excitation from the S_0 state to the S_1 state, as verified by the RMSD analysis (Figure S2). According to the calculated results shown in Table 1, the C1−C2, C2−C3, C3−C4, C5−C6, and C6−C1 bonds in the benzene ring become a little longer upon excitation while the C4−C5 bond stays about the same for the *cis*-rotamer; for the *trans*-rotamer, the C1−C2, C2−C3, C4−C5, and C5−C6 bonds become longer during the $S_1 \leftarrow S_0$ transition, while the C3−C4 and C6−C1 bonds are contracted by 0.001 and 0.006 Å, respectively. The above observations are consistent with the previous studies, which showed that the $S_1 \leftarrow S_0$ transitions of benzene derivatives are mainly subject to the $\pi^* \leftarrow \pi$ electronic excitation and a benzene ring distortion usually occurs, making it deviate from a perfect hexagon.[31,32] Such transition scheme is confirmed by analyzing the molecular orbitals involved in the first electronic transition (Figure S3).

Besides the benzene ring distortion, the C3−Cl bond connecting the benzene ring and the Cl atom is shortened by 0.009 Å for the *cis*-rotamer during the $S_1 \leftarrow S_0$ transition, while it is elongated slightly by 0.007 Å for the *trans*-rotamer. This may indicate that the steric effect between the Cl atom and the $-SCH_3$ group becomes weaker and/or the interaction between the Cl atom and the benzene ring becomes stronger in the S_1 state for the *cis*-rotamer. The $-SCH_3$ group is also distorted during the $S_1 \leftarrow S_0$ transition. The S−C1 bond connecting the $-SCH_3$ group with the benzene ring is shortened by 0.020 Å for the *cis*-rotamer and 0.021 Å for the *trans*-rotamer. The S−C8 bond connecting the S atom with the $-CH_3$ group is shortened by 0.011 Å for the *cis*-rotamer and 0.009 Å for the *trans*-rotamer. This is consistent with the change of the intramolecular charge distribution upon photoexcitation. As shown in Table 1, all H atoms in the $-CH_3$ group and the S atom become more positive upon the excitation, while all H atoms directly connected to the benzene ring, and all of the C atoms of the benzene ring become more negative in the S_1 state, except for C4, which becomes less negative and is furthest from the $-SCH_3$ group. The shortened bond lengths and the intramolecular charge distribution changes in the S_1 state enhance the $p-\pi$ conjugation interaction between the $-SCH_3$ group and the benzene ring (Figure S3). Some anisole

https://doi.org/10.1021/acsomega.1c06003
ACS Omega 2022, 7, 8456−8465

derivatives, such as 3-F anisole[21] and 3-Cl anisole,[23] undergo similar ring deformation upon excitation from the S_0 state to the S_1 state.

3.1.3. Structural Changes during Photoionization. Both the measured spectra and theoretical calculations suggest that both of the 3ClTA rotamers adopt a stable planar structure in the D_0 state. The calculated results show that for both rotamers, the benzene ring of 3ClTA has longer C1−C2, C3−C4, C4−C5, and C6−C1 bonds and shorter C2−C3 and C5−C6 bonds in the D_0 state than those in the S_0 state, showing a quinoidal structure. The chlorine atom and all the C atoms of the benzene ring except for C1 that connects with the $-SCH_3$ group become more positive (or less negative) in the D_0 state than those in the S_1 state upon photoionization; while the changes of the charges on C1 and the $-SCH_3$ group are comparably smaller. This implies that the ejected photoelectron is mainly contributed by the nonbonding *p* orbitals of the S and Cl atoms and the π orbital of the benzene ring (see the plotted highest molecular orbitals in Figure S3).

For the $-SCH_3$ group, the S−C1 bond shows a very strong double bond character in the D_0 state, and it is significantly shorter (1.718 Å for the *cis*-rotamer and 1.716 Å for the *trans*-rotamer) than that in S_0 (1.774 Å for the *cis*-rotamer and 1.775 Å for the *trans*-rotamer) and S_1 states (1.754 Å for the *cis*-rotamer and 1.754 Å for the *trans*-rotamer). This is consistent with the spectroscopic measurements that the frequencies of the methyl torsion mode τ^1 for both rotamers become significantly larger in the D_0 state (88 cm^{-1} for the *cis*-rotamer and 34 cm^{-1} for the *trans*-rotamer) than those in the S_1 state (46 cm^{-1} for the *cis*-rotamer and 24 cm^{-1} for the *trans*-rotamer). The above observations indicate that the conjugation interaction between the *p* orbital occupied by the remaining nonbonding electron on the S atom and the π orbital on the benzene ring is enhanced in the photoionization process.

For the Cl atom, the C3−Cl bond is also significantly shorter in the D_0 state (1.719 Å for the *cis*-rotamer and 1.722 Å for the *trans*-rotamer) than that in S_0 (1.755 Å for the *cis*-rotamer and 1.754 Å for the *trans*-rotamer) and S_1 states (1.746 Å for the *cis*-rotamer and 1.761 Å for the *trans*-rotamer). The Cl atom can interact with the benzene ring through the *p*-π conjugative effect, which arises from the donation of a lone pair electron from the Cl atom to the benzene ring, thus the conjugative effect between the Cl atom and the benzene ring may also be enhanced due to the shortened C3−Cl bond in the D_0 state and the rigidity of the benzene ring could be increased. This is in accordance with the spectroscopic observations. For example, the frequencies of the in-plane ring deformation mode 1^1 in the D_0 state (980 cm^{-1} for the *cis*-rotamer and 981 cm^{-1} for the *trans*-rotamer) are slightly larger than those in the S_1 state (953 cm^{-1} for the *cis*-rotamer and 963 cm^{-1} for the *trans*-rotamer), indicating a more rigid benzene ring in the D_0 state.

3.2. Active Vibrational Modes and Their Frequencies. The present 1C-R2PI and MATI spectroscopic measurements show that the in-plane ring deformation modes $6a_0^1$, ν_s^1, and 1_0^1 of the *cis*-rotamer have frequencies of 349, 617, and 953 cm^{-1} in the S_1 state, and, respectively, become 366 (or 398), 652, and 980 cm^{-1} in the D_0 state; the in-plane ring deformation mode 1_0^1 of the *trans*-rotamer has a frequency of 963 cm^{-1} in the S_1 state, and becomes 981 cm^{-1} in the D_0 state. Thus, almost all of the benzene ring-related vibrational modes have higher frequencies for both the *cis*- and *trans*-rotamers during the photoionization process, indicating that the conjugation effects between the benzene ring and the substituent groups are enhanced in the D_0 state. This increases the rigidity of the benzene ring. Similar vibrational frequency enhancement by photoionization was observed for the substituent-sensitive modes, for example, the methyl torsion mode τ_0^1, as presented above.

The current study along with several previous studies on other anisole derivatives[21,23,27,30] and TA derivatives[6,11] show that the frequencies of the benzene-ring-related modes are not very sensitive to the orientations of the substituents. In this study, the frequencies of the substituent-sensitive modes, e.g., the methyl torsion mode τ_0^1, are measured for both the *cis*- and *trans*-3ClTA. Its frequency for the *cis*-rotamer is 46 cm^{-1} in the S_1 state, and 88 cm^{-1} in the D_0 state, while it is only 24 and 34 cm^{-1} in the S_1 and D_0 states of the *trans*-rotamer. The MATI spectra *via* the methyl torsion mode τ_0^1 for the two rotamers as shown in Figure 7a,e show that the coupling scheme of the methyl torsion mode τ_0^1 to other vibrational modes is strongly rotamer-dependent. This may be caused by the different through-space interactions between the two substituents Cl and $-SCH_3$ in the two rotamers. The two substituents are closer to each other, and thus should have stronger through-space interaction in the *cis*-rotamer than that in the *trans*-rotamer. That makes the methyl group in the *cis*-rotamer harder to move, resulting in a larger vibrational frequency.

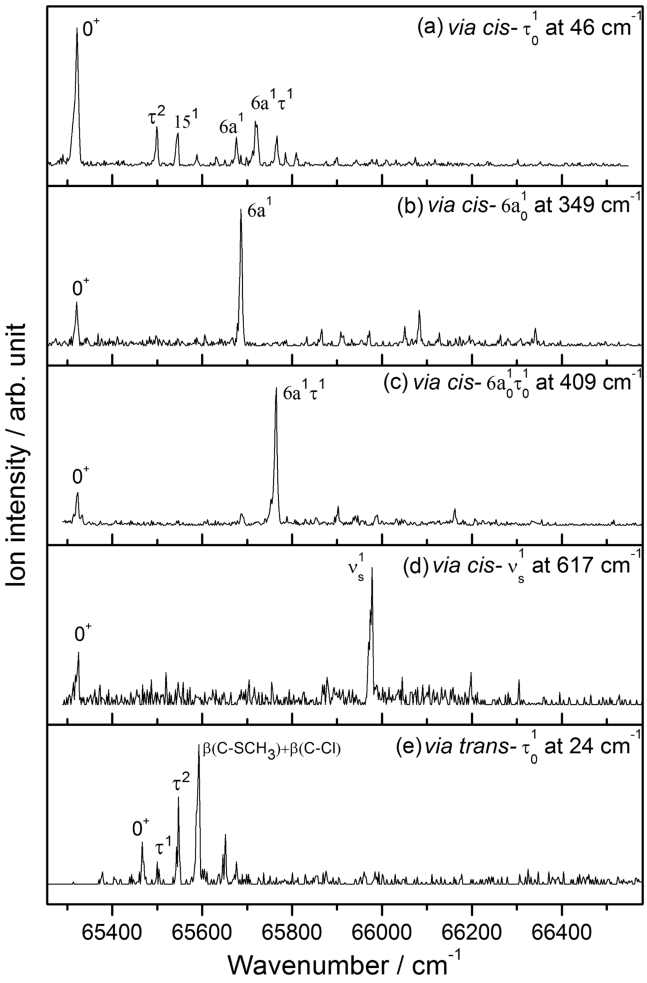

Figure 7. MATI spectra of *cis*- and *trans*-^{35}Cl-3ClTA recorded *via* different vibrational modes in the S_1 state.

https://doi.org/10.1021/acsomega.1c06003
ACS Omega 2022, 7, 8456−8465

Table 4. Transition and Ionization Energies (in cm^{-1}) of Anisole and TA Derivatives

	E_1	ΔE_1	IE	ΔIE		E_1	ΔE_1	IE	ΔIE
thioanisole (TA)[a]	34 506		63 906		anisole	36 383[d]	0	66 399[e]	
trans-o-fluorothioanisole[b]	34 974	468	65 114	1208	*trans-o*-fluoroanisole[f]	36 611	228	67 354	955
cis-m-fluorothioanisole[c]	34 820	314	65 468	1562	*cis-m*-fluoroanisole[g]	36 662	279	67 867	1468
trans-m-fluorothioanisole[c]	35 047	541	64 644	1738	*trans-m*-fluoroanisole[g]	36 819	436	68 304	1905
cis-m-chlorothioanisole	33 959	−547	65 326	1420	*cis-m*-chloroanisole[i]	35 822	−561	67 645	1246
	(33 580)[h]		(63 205)[h]						
trans-m-chlorothioanisole	34 102	−404	65 471	1565	*trans-m*-chloroanisole[i]	35 868	−515	68 008	1609
	(33 434)[h]		(63 456)[h]						

[a]From ref 6. [b]From ref 11. [c]From our unpublished data. [d]From ref 2 [e]From ref 44. [f]From ref 17. [g]From ref 21. [h]Values in parentheses represent theoretical values calculated in this work. [i]From ref 23.[23]

It should also be noted that the methyl torsion mode τ_0^1 has been observed to be active in TA,[6,9,12] *trans*-2FTA,[11] and *cis*- and *trans*-3ClTA, while it was not observed for stable anisole derivatives, such as 2-F anisole,[22] 3-Cl anisole,[23] and 3-F anisole.[21] This indicates that the methyl group on the more flexible $-SCH_3$ group is easier to be activated.

3.3. Substitution Effect on the Electronic Excitation and Ionization Energies. The measured electronic excitation transition energies (E_1) and ionization energies (IE) of several anisole and TA derivatives are listed in Table 4. It can be seen that the E_1 and IE values depend on both the nature and location of the substituent halogen atom.

For E_1 values shown in Table 4, the E_1 values of the Cl-substituted TA derivatives, *cis*- and *trans*-3ClTA, are red-shifted by 547 and 404 cm^{-1}, respectively, relative to that of TA,[6,9,12] while the E_1 values of the F-substituted TA derivatives, the *trans*-2FTA,[11] and *cis*- and *trans*-3FTA, are all blue-shifted compared to that of TA.[6,9,12] Similar phenomena have been observed between anisole and its F- and Cl-substituted derivatives.[2,17,21,23] A previous study showed that the substitution of a functional group on the benzene ring can lower its zero-point energy (ZPE) level.[21] The red-shifted E_1 values of 3ClTA imply that the interaction of Cl with the benzene ring is stronger in the S_1 state than that in the S_0 state, resulting in a larger ZPE lowering of the S_1 state than that of the S_0 state.

4. CONCLUSIONS

The 1C-R2PI and MATI spectra of *cis*- and *trans*-3ClTA are obtained, implying that both the *cis*- and *trans*-rotamers coexist in the experiment and have planar structures in their respective S_0, S_1, and D_0 states. The *cis*-rotamer is slightly more stable than the *trans*-rotamer with an isomerization barrier of ∼500 cm^{-1}. The first electronic excitation and ionization energies of *cis*-3ClTA are determined to be 33 959±3 and 65 326±5 cm^{-1}, and those of *trans*-3ClTA to be 34 102±3 and 65 471±5 cm^{-1}, respectively. The two Cl isotopes are found to have negligible effects on the molecular properties of 3ClTA. The E_1 and IE values are red-shifted by the Cl substitution for both rotamers, similar to the anisole derivatives.

Most of the active vibrations are found to be the in-plane ring deformation and substituent-sensitive modes. Their vibrational frequencies are generally measured to be higher in the D_0 state than those in the S_1 state, indicating that the conjugation interaction between the benzene ring and the substituted functional groups and the through-space interaction between the two substituents are enhanced during the photoionization process. This is confirmed by the molecular structural changes due to photoionization as revealed by theoretical calculations. The frequencies of the in-plane ring deformation modes are found to be not sensitive to the relative orientation between the two substituents, while the frequencies of the substituent-sensitive modes and their coupling schemes with other vibrational modes are found to be strongly rotamer-dependent.

5. EXPERIMENTAL AND COMPUTATIONAL METHODS

5.1. Experimental Methods. The photoionization time-of-flight (TOF) mass spectrometer used in the current study has been described previously,[5,20] and only a brief description is given here. The 3ClTA sample with a purity of 99% was purchased from Alfa Aesar and used without further purification. It was seeded in the Ar carrier gas (∼2 atm) and then expanded into a vacuum chamber through a pulsed General valve with a nozzle diameter of 0.25 mm. The molecular beam passed through a skimmer with a diameter of 1 mm located at 20 mm downstream from the nozzle and then entered the photoionization region of the mass spectrometer, which is 70 mm from the nozzle. In the photoionization region, the molecular beam was crossed by one or two ultraviolet (UV) laser beams perpendicularly and photoionized for detection.

In the one color resonant two-photon ionization (1C-R2PI) spectroscopic measurement, only one UV laser beam was used. The 3ClTA molecule absorbed a single UV photon to be excited to the S_1 state first, and then the 3ClTA molecule in the S_1 state absorbed a second UV photon to go above the photoionization threshold. The ions thus produced by the UV laser were immediately accelerated by two direct-current electric fields of 200 and 2100 V/cm, respectively. In the MATI experiment, two counterpropagating UV laser beams of different wavelengths were used. The first UV laser beam was the same as that used in the 1C-R2PI experiment and was used to excite the 3ClTA molecule to its S_1 state; the second UV beam excited the molecules from the S_1 state to the high-*n*-Rydberg states, which are slightly below the ionization thresholds. The photoionization region was field-free during the photoexcitation process, and after about 200 ns, a pulsed electric field of −0.5 V/cm was switched on to reject the prompt ions, which were usually generated together with the high-*n*-Rydberg neutrals. After a delay of 11 μs, two pulsed electric fields of +200 and +2000 V/cm were switched on synchronously to field ionize the high-*n*-Rydberg neutrals and accelerate the produced ions to the detector. The ions produced in the above two processes were focused by an Einzel lens and flew through a 1.0 m long field-free tube toward a dual-stacked microchannel plate (MCP) detector.

https://doi.org/10.1021/acsomega.1c06003
ACS Omega 2022, 7, 8456−8465

After passing through a preamplifier (SR445, Stanford Research System), the TOF signal was amplified by 25 times and collected by a multichannel scaler (SR430, Stanford Research System).

The UV lasers used in this experiment were generated by doubling the outputs of two tunable dye lasers (Sirah-CSTR), which were pumped by the second harmonic output of an Nd:YAG laser (Quanta-Ray, Pro-230-10E) at a repetition rate of 10 Hz. Three laser dyes, Pyrromethene 597, Pyrromethene 580, and DCM, were used in this work. Two pulse delay generators (DG535, Stanford Research System) were used to synchronize the whole system. Typical pressures of $\sim 3.0 \times 10^{-3}$ and $\sim 3.0 \times 10^{-5}$ Pa were maintained in the source and ionization chambers during operation.

5.2. Computational Methods. All calculations in this study were carried out with the Gaussian09 program package.[33] The stable structures and harmonic vibrational frequencies of 3ClTA in S_0, S_1, and D_0 states were calculated with density functional theory (DFT), in which time-dependent DFT (TDDFT)[34,35] was used for the excited state S_1. The B3LYP functional[36,37] and cc-pVTZ basis set[38−40] were employed for all the calculations, and no imaginary frequencies were found for the optimized stationary points. The relaxed potential energy curve (PEC) in the S_0 state was scanned to illustrate the isomerization barrier between the *cis*- and *trans*-3ClTA. The calculated vibrational frequencies of 3ClTA in S_0, S_1, and D_0 states were scaled by 0.967[41] to approximately account for the vibrational anharmonicity effect. The charge distributions based on natural population analysis (NPA)[42] were conducted by Natural Bond Orbital (NBO) version 3.1 program implemented in the Gaussian09 program package.[43]

■ ASSOCIATED CONTENT

Supporting Information

The Supporting Information is available free of charge at https://pubs.acs.org/doi/10.1021/acsomega.1c06003.

Vibrational vectors of selected modes (Figure S1), overlaid structures and RMSD values for distances (Figure S2), molecular orbitals (Figure S3), Cartesian coordinates (Table S1), and numerical data of Figures 4−7 (Tables S2−S5) (PDF)

■ AUTHOR INFORMATION

Corresponding Authors

Yikui Du − *Beijing National Laboratory for Molecular Sciences (BNLMS), Institute of Chemistry, Chinese Academy of Sciences, Beijing 100190, China; University of Chinese Academy of Sciences, Beijing 100049, China;* orcid.org/0000-0001-7910-8257; Email: ydu@iccas.ac.cn

Gao-Lei Hou − *MOE Key Laboratory for Non-Equilibrium Synthesis and Modulation of Condensed Matter, School of Physics, Xi'an Jiaotong University, Xi'an 710049 Shaanxi, China;* orcid.org/0000-0003-1196-2777; Email: gaolei.hou@xjtu.edu.cn

Hong Gao − *Beijing National Laboratory for Molecular Sciences (BNLMS), Institute of Chemistry, Chinese Academy of Sciences, Beijing 100190, China; University of Chinese Academy of Sciences, Beijing 100049, China;* orcid.org/0000-0002-6168-7630; Email: honggao2017@iccas.ac.cn

Author

Zhe Zhang − *Beijing National Laboratory for Molecular Sciences (BNLMS), Institute of Chemistry, Chinese Academy of Sciences, Beijing 100190, China; University of Chinese Academy of Sciences, Beijing 100049, China*

Complete contact information is available at: https://pubs.acs.org/10.1021/acsomega.1c06003

Notes

The authors declare no competing financial interest.

■ ACKNOWLEDGMENTS

This work was supported by the Program for Young Outstanding Scientists of Institute of Chemistry, Chinese Academy of Science (ICCAS), and Beijing National Laboratory for Molecular Sciences (BNLMS). Computational resources and services were provided by the VSC (Flemish Supercomputer Center), funded by the Research Foundation-Flanders (FWO) and the Flemish Government-department EWI, and part of the theoretical calculations was also conducted on the China Scientific Computing Grid (ScGrid) of the Supercomputing Center, Computer Network Information Center of the Chinese Academy of Sciences. G.-L. Hou acknowledges the start-up support of Xi'an Jiaotong University via the "Young Talent Support Plan".

■ REFERENCES

(1) Huang, H. C.; Jin, B. Y.; Tzeng, W. B. Two-color resonant two-photon ionization and mass-analyzed threshold ionization spectroscopy of o-chloroanisole. *J. Photochem. Photobiol., A* **2012**, *243*, 73−79.

(2) Eisenhardt, C. G.; Gemechu, A. S.; Baumgärtel, H.; Chelli, R.; Cardini, G.; Califano, S. Excited state photoelectron spectroscopy of anisole. *Phys. Chem. Chem. Phys.* **2001**, *3*, 5358−5368.

(3) Yu, D.; Dong, C. W.; Zhang, L. J.; Cheng, M.; Hu, L. L.; Du, Y. K.; Zhu, Q. H.; Zhang, C. H. Resonant two-photon ionization spectroscopy of the ^{35}Cl and ^{37}Cl isotopomers of cis and trans 3-chloro-4-fluoroanisole. *J. Mol. Struct.* **2011**, *1000*, 92−98.

(4) Yamakita, Y.; Okazaki, T.; Ohno, K. Conformation-Specific Raman Bands and Electronic Conjugation in Substituted Thioanisoles. *J. Phys. Chem. A* **2008**, *112*, 12220−12227.

(5) Xiao, D. Q.; Yu, D.; Xu, X. L.; Yu, Z. J.; Du, Y. K.; Gao, Z.; Zhu, Q. H.; Zhang, C. H. Vibrational spectrum of p-fluoroanisole in the first excited state (S_1) and ab initio calculations. *J. Mol. Struct.* **2008**, *882*, 56−62.

(6) Vondrák, T.; Sato, S.; Spirko, V.; Kimura, K. Zero kinetic energy (ZEKE) photoelectron spectroscopic study of thioanisole and its van der Waals complexes with argon. *J. Phys. Chem. A* **1997**, *101*, 8631−8638.

(7) Lunazzi, L.; Macciantelli, D. Conformational dependence of long-range coupling in ortho-substituted thioanisoles. *J. Chem. Soc. D* **1971**, 933−934.

(8) Lim, J. S.; Kim, S. K. Experimental probing of conical intersection dynamics in the photodissociation of thioanisole. *Nat. Chem.* **2010**, *2*, 627−632.

(9) Li, S. L.; Xu, X.; Truhlar, D. G. Computational simulation and interpretation of the low-lying excited electronic states and electronic spectrum of thioanisole. *Phys. Chem. Chem. Phys.* **2015**, *17*, 20093−20099.

(10) Isozaki, T.; Sakeda, K.; Suzuki, T.; Ichimura, T.; Tsuji, K.; Shibuya, K. Evidence for a non-planar conformer and conformational isomerization of o-fluoroanisole in a low-temperature Ar matrix. *Chem. Phys. Lett.* **2005**, *409*, 93−97.

(11) Lim, J. S.; You, H. S.; Kim, S. Y.; Kim, S. K. Experimental observation of nonadiabatic bifurcation dynamics at resonances in the continuum. *Chem. Sci.* **2019**, *10*, 2404−2412.

(12) Shishkov, I. F.; Khristenko, L. V.; Karasev, N. M.; Vilkov, L. V.; Oberhammer, H. Structure and conformation of thioanisole: Gas electron diffraction and contradicting quantum chemical calculations. *J. Mol. Struct.* **2008**, *873*, 137−141.
(13) Li, S. L.; Truhlar, D. G. Full-dimensional multi-state simulation of the photodissociation of thioanisole. *J. Chem. Phys.* **2017**, *147*, 044311.
(14) Li, S. L.; Truhlar, D. G. Full-dimensional ground- and excited-state potential energy surfaces and state couplings for photodissociation of thioanisole. *J. Chem. Phys.* **2017**, *146*, 064301.
(15) Zaripov, N. M. Electron diffraction study of the structure of the thioanisole molecule. *J. Struct. Chem.* **1976**, *17*, 640−642.
(16) Liu, S.; Zhang, L. J.; Dai, W. S.; Cheng, M.; Du, Y. K.; Zhu, Q. H. REMPI and MATI spectroscopy of cis and trans 3-chloro-N-methylaniline. *J. Mol. Spectrosc.* **2017**, *336*, 12−21.
(17) Shiung, K. S.; Yu, D.; Tzeng, S. Y.; Tzeng, W. B. Cation spectroscopy of o-fluoroanisole and p-fluoroanisole by two-color resonant two-photon mass-analyzed threshold ionization. *Chem. Phys. Lett.* **2012**, *524*, 38−41.
(18) Tzeng, W. B.; Narayanan, K.; Hsieh, C. Y.; Tung, C. C. Structures and vibrations of ortho-, meta-, and para-fluoroanilines in the S0 and S1 states by ab initio calculations and resonant two-photon ionization spectroscopy. *J. Chem. Soc., Faraday Trans.* **1997**, *93*, 2981−2987.
(19) Marchetti, B.; Karsili, T. N. V.; Cipriani, M.; Hansen, C. S.; Ashfold, M. N. R. The near ultraviolet photodissociation dynamics of 2-and 3-substituted thiophenols: Geometric vs. electronic structure effects. *J. Chem. Phys.* **2017**, *147*, 013923.
(20) Dong, C. W.; Zhang, L. J.; Liu, S.; Hu, L. L.; Cheng, M.; Du, Y. K.; Zhu, Q. H.; Zhang, C. H. REMPI and MATI spectroscopic study of selected cis and trans 3-chlorostyrene rotamers. *J. Mol. Spectrosc.* **2013**, *292*, 35−46.
(21) Shiung, K. S.; Yu, D.; Huang, H. C.; Tzeng, W. B. Rotamers of m-fluoroanisole studied by two-color resonant two-photon mass-analyzed threshold ionization spectroscopy. *J. Mol. Spectrosc.* **2012**, *274*, 43−47.
(22) Isozaki, T.; Sakeda, K.; Suzuki, T.; Ichimura, T. Fluorescence spectroscopy of jet-cooled o-fluoroanisole: Mixing through Duschinsky effect and Fermi resonance. *J. Chem. Phys.* **2010**, *132*, 214308.
(23) Huang, H. C.; Shiung, K. S.; Jin, B. Y.; Tzeng, W. B. Rotamers of m-chloroanisole studied by two-color resonant two-photon mass-analyzed threshold ionization spectroscopy. *Chem. Phys.* **2013**, *425*, 114−120.
(24) Ingemann, S.; Nibbering, N. M. M. Gas-phase reactions of anions with 2-, 3-, and 4-fluoroanisole. *J. Org. Chem.* **1983**, *48*, 183−191.
(25) Zhang, L. J.; Dong, C. W.; Cheng, M.; Hu, L. L.; Du, Y. K.; Zhu, Q. H.; Zhang, C. H. Resonance-enhanced two-photon ionization spectroscopy and theoretical calculations of 3,5-difluoroanisole and its Ar-containing complex. *Spectrochim. Acta, Part A* **2012**, *96*, 578−585.
(26) Dai, W. S.; Zhang, Z.; Du, Y. K. R2PI and MATI spectroscopy of 3-fluoro-5-methylanisole: Combined effect of meta-substituents on molecular conformation. *Spectrochim. Acta, Part A* **2020**, *224*, 117398.
(27) Lo, K. W.; Tzeng, W. B. 3-Chloro-4-fluoroaniline studied by resonant two-photon ionization and mass-analyzed threshold ionization spectroscopy. *J. Mol. Spectrosc.* **2013**, *288*, 1−6.
(28) Huang, W. C.; Yeh, W. L.; Tzeng, W. B. Vibronic and cation spectroscopy of m-chloroaniline. *J. Mol. Spectrosc.* **2011**, *269*, 248−253.
(29) Varsányi, G. *Assignments for Vibrational Spectra of Seven Hundred Benzene Derivatives*; Wiley: New York, 1974; p 214.
(30) Chen, Q.; Tzeng, S. Y.; Zhang, B.; Tzeng, W. B. Rotamers of m-Methylanisole Studied by Mass-Analyzed Threshold Ionization Spectroscopy. *Acta Phys.-Chim. Sin.* **2014**, *30*, 1416−1425.
(31) Lin, J. L.; Tzeng, W. B. Mass analyzed threshold ionization of deuterium substituted isotopomers of aniline and p-fluoroaniline: Isotope effect and site-specific electronic transition. *J. Chem. Phys.* **2001**, *115*, 743−751.
(32) Huang, K. T.; Lombardi, J. R. Dipole moment of lowest singlet $\pi^*\leftarrow\pi$ states in p-fluorophenol and p-fluoroaniline. *J. Chem. Phys.* **1969**, *51*, 1228.
(33) Frisch, M. J.; Trucks, G. W.; Schlegel, H. B.; Scuseria, G. E.; Robb, M. A.; Cheeseman, J. R.; Scalmani, G.; Barone, V.; Mennucci, B.; Petersson, G. A.; Nakatsuji, H.; Caricato, M.; Li, X.; Hratchian, H. P.; Izmaylov, A. F.; Bloino, J.; Zheng, G.; Sonnenberg, J. L.; Hada, M.; Ehara, M.; Toyota, K.; Fukuda, R.; Hasegawa, J.; Ishida, M.; Nakajima, T.; Honda, Y.; Kitao, O.; Nakai, H.; Vreven, T.; Montgomery, J. A., Jr.; Peralta, J. E.; Ogliaro, F.; Bearpark, M.; Heyd, J. J.; Brothers, E.; Kudin, K. N.; Staroverov, V. N.; Kobayashi, R.; Normand, J.; Raghavachari, K.; Rendell, A.; Burant, J. C.; Iyengar, S. S.; Tomasi, J.; Cossi, M.; Rega, N.; Millam, J. M.; Klene, M.; Knox, J. E.; Cross, J. B.; Bakken, V.; Adamo, C.; Jaramillo, J.; Gomperts, R.; Stratmann, R. E.; Yazyev, O.; Austin, A. J.; Cammi, R.; Pomelli, C.; Ochterski, J. W.; Martin, R. L.; Morokuma, K.; Zakrzewski, V. G.; Voth, G. A.; Salvador, P.; Dannenberg, J. J.; Dapprich, S.; Daniels, A. D.; Farkas, Ö.; Foresman, J. B.; Ortiz, J. V.; Cioslowski, J.; Fox, D. J. *Gaussian 09*, revision C.01; Gaussian Inc.: Wallingford CT, 2010.
(34) Bauernschmitt, R.; Ahlrichs, R. Treatment of electronic excitations within the adiabatic approximation of time dependent density functional theory. *Chem. Phys. Lett.* **1996**, *256*, 454−464.
(35) Adamo, C.; Jacquemin, D. The calculations of excited-state properties with Time-Dependent Density Functional Theory. *Chem. Soc. Rev.* **2013**, *42*, 845−856.
(36) Becke, A. D. Density-functional thermochemistry. III. the role of exact exchange. *J. Chem. Phys.* **1993**, *98*, 5648−5652.
(37) Lee, C. T.; Yang, W. T.; Parr, R. G. Development of the colle-salvetti correlation-energy formula into a functional of the electron-density. *Phys. Rev. B* **1988**, *37*, 785−789.
(38) Dunning, T. H. Gaussian-basis sets for use in correlated molecular calculations. I. the atoms boron through neon and hydrogen. *J. Chem. Phys.* **1989**, *90*, 1007−1023.
(39) Woon, D. E.; Dunning, T. H. Gaussian-basis sets for use in correlated molecular calculations. III. the atoms aluminum through argon. *J. Chem. Phys.* **1993**, *98*, 1358−1371.
(40) Pritchard, B. P.; Altarawy, D.; Didier, B.; Gibson, T. D.; Windus, T. L. New Basis Set Exchange: An Open, Up-to-Date Resource for the Molecular Sciences Community. *J. Chem Inf. Model.* **2019**, *59*, 4814−4820.
(41) Available online: https://cccbdb.nist.gov/vibscalejust.asp (accessed on December 31, 2021).
(42) Reed, A. E.; Weinstock, R. B.; Weinhold, F. Natural-population analysis. *J. Chem. Phys.* **1985**, *83*, 735−746.
(43) Glendening, E. D.; Reed, A. E.; Carpenter, J. E.; Weinhold, F., NBO Version 3.1.
(44) Pradhan, M.; Li, C. Y.; Lin, J. L.; Tzeng, W. B. Mass analyzed threshold ionization spectroscopy of anisole cation and the OCH3 substitution effect. *Chem. Phys. Lett.* **2005**, *407*, 100−104.

https://doi.org/10.1021/acsomega.1c06003
ACS Omega 2022, 7, 8456−8465